ESKİŞEHİR TECHNICAL UNIVERSITY JOURNAL OF SCIENCE AND TECHNOLOGY
A- APPLIED SCIENCES AND ENGINEERING

2023, 24(1), pp. 14-22, DOI:10.18038/estubtda.912081

RESEARCH ARTICLE

PHOTOLUMINESCENCE PROPERTIES OF Nd^{3+}, Yb^{3+} CODOPED Ga_2O_3 NANOPARTICLES

Ayşe DULDA *

Department of Material Science and Nanotechnology Engineering, Engineering Faculty, Yeditepe University, İstanbul, Turkey

ABSTRACT

The availability of sensitive photon detectors and inexpensive lasers allowed us to explore more efficient fluorescent probes that will work in second near-infrared optical window. In this study, the optical properties of Nd^{3+} and Yb^{3+} co-doped Ga_2O_3 nanoparticles were studied. In order to indicate the correlation between particle size, crystallinity and optical property of present samples XRD, TEM, and Photoluminescence analyses were performed. Various excitation wavelengths and dopant concentrations were used to understand the energy transfer mechanism in Nd^{3+} and Yb^{3+} co-doped Ga_2O_3 nanoparticles. As the excitation wavelength increased from 325 nm to 477 and 515 nm, Yb^{3+} emission peak intensity decreased while Nd^{3+} emission peak intensity increased. This inverse relationship between the emission intensities of Yb^{3+} and Nd^{3+} ion showed the presence of energy transfer between them. Resulting emission peaks were broad and weak, indicating the presence of a non-radiative decay channel due to the crystal defects.

Keywords: Energy Transfer, Gallium Oxide, Nd^{3+}, Yb^{3+}, Near Infrared Emission, Luminescence

1. INTRODUCTION

One of the most important issue that researchers work on is the ability of monitoring biological structures and their functioning at the molecular level. Among the other bioimaging techniques fluorescence microscopy offers a unique approach for visualizing morphological details in tissue with subcellular resolution [1,2] In recent decades, upconversion nanoparticles (UCNPs) frequently preferred over other commercial fluorescent probes such as quantum dots, metal complexes and dye molecules because of many advantages [3] . These UCNPs composed of rare earths that emit radiations from visible (400–700 nm) to near-infrared (NIR-I, 750–900 nm) regions of the electromagnetic spectrum. However, the limited penetration depth of light in tissue (1–2 mm) leads to extension of biological window to 1000-1700 nm (NIR-II window)[4–9] . In addition, the advances in optoelectronic technology such as fabrication of sensitive cameras (InGaAs and HgCdTe cameras), fiber optics, and diode lasers have allowed us to shift our working area to the second near-infrared window [4]Lim et al. have reported that 1000-fold improvement in fluorescence imaging quality in the NIR-II window [10].

Diao, S. et al. have shown that auto-fluorescence free emission over 1500 nm (NIR-II window) [11]. Wang et al. have developed a fluorescent probe emitting at 1525 nm that achieves high penetration depth (18 mm), even detectable with a low concentration of 5 nM [12]. Those are the extrinsic effects influencing penetration depth as a result of light interaction with tissue (absorbance, scattering and autofluorescence). Intrinsic properties of fluorescence probe (host materials and defects) are also important for prob efficiency, hence image quality.

*Corresponding Author: ayse.dulda@yeditepe.edu.tr
Received: 08.04.2021 Published: 29.03.2023

In our previous study, over thousand nanometer emission from Nd^{3+} and Yb^{3+} co-doped Ga_2O_3 nanoparticles reported under NIR excitations. Nd^{3+} and Yb^{3+} were selected as dopants as the transitions between (Nd^{3+}: $^4F_{3/2}\rightarrow{}^4I_{9/2}$) and ($Yb^{3+}$: $^2F_{7/2}\rightarrow{}^2F_{5/2}$) energy levels highly overlap for efficient energy transfer [13,14] . Here excitations in the visible range is studied to understand the effect of defects on the energy transfer mechanism and the optical property of present sample. To the best of our knowledge, although there are many lanthanides doped Ga_2O_3 have been reported in literature, this study will be the first investigating energy transfer in Nd^{3+} and Yb^{3+} co-doped Ga_2O_3 system.

2. MATERIALS and METHODS

2.1. Chemicals

$GaCl_3$ (ultra dry 99,999% Abcr), $YbCl_3$ (Ytterbium(III) chloride anhydrous, -10 mesh, 99.99%, Sigma Aldrich), $NdCl_3$, Neodymium(III) chloride hexahydrate (99.9% trace metals basis, Sigma Aldrich), oleic acid (97%, ACROS Organics), sodium oleate(≥82% fatty acids (as oleic acid) basis, Sigma Aldrich) and 1-Octadecene (90%, tech., ACROS Organics) were used without further purification, n-hexane, ethanol.

2.2. Procedure

2.2.1. Synthesis of metal-oleate complex

Yb^{3+} and Nd^{3+} codoped Ga_2O_3 nanocrystals were prepared by thermal decomposition method[15] . In a typical synthesis, 10 mmol metal chlorides (%99,4 or %99,5 $GaCl_3$, %0,4, or %0,5 $YbCl_3$, %0,1 $NdCl_3$) and sodium oleate (20 mmol) were dissolved in a mixture of solvents of ethanol (10 mmol), hexane (17,5 mmol) and deionised water (7,5 mmol) by stirring in a heating mantle. This mixture heated to 60°C and kept at this temperature for 4 hours in inert atmosphere. The resulting solution was in two phase. Upper organic phase containing metal oleate complex was separated via separating funnel and the metal oleate complex washed several times. The resulting waxy solution was left in an oven at 100°C to allow the remaining solvent (hexane and water) to be completely evaporated off.

2.2.2.Synthesis of Nd3+, Yb3+ doped Ga2O3 nanoparticles

The final organic complex (2 mmol metal oleate) was heated to 320 °C in a mixture of 10 g octadecene and 1mmol oleic acid with a heating rate of 2 °C/min. and then maintained for one hour at this temperature. When the reaction is completed resulting particles were washed with hexane and ethanol to separate organics from nanoparticles through centrifugation.

2.3. Instumentations

The crystalline phases of the samples were determined by powder X-Ray Diffraction method using a Bruker D8 Advance X-ray diffractometer with CuKα radiation. The scan rate of 2θ°/min was set over the range of 10 – 70°. The morphological characterization of the samples was monitored using transmission electron microscopy (FE-TEM, 200 kV, Tecnai F20). Samples were prepared for TEM investigations by putting an aliquot of n-hexane solution of nanoparticles onto an amorphous carbon substrate supported on a copper grid. X-ray diffraction analyses were carried out using Micro-area X-ray diffractometer (Rigaku, D/MAX-2500). The room temperature photoluminescence (PL) spectrum of the powder samples was measured using a grating monochromator and a thermo-electrically cooled InGaAs photodiodes for the IR region employing the standard lock-in technique. The 325 nm line of a He-Cd laser (10 mW) and the 477 and 515 nm lines of an Ar laser (200 mW) were used as excitation sources. All spectrum results were corrected for the system response.

3. RESULTS and DISCUSSIONS

3.1. Morphology and Crystallinity

The crystalline structures and phase purities of Ga_2O_3:Yb^{3+}, Nd^{3+} sample prepared through the thermal decomposition method is examined by XRD. Figure 1 shows the XRD pattern of Ga_2O_3: $Nd_{0,1}$, $Yb_{0,5}$ nanoparticles. The diffraction peaks agree with the XRD pattern of Gallium oxide registered in JCPDS card No: 43-1011 with a monoclinic crystal structure in the space group c2/m and lattice parameters are a = 12.23 Å, b = 3.04 Å, c = 5.80 Å and β= 103.7Å [16] . The resulting peaks are sharp, indicating the high crystallinity of the present sample. Since a small amount of lanthanide ion is added, it does not cause any peak shifts or an additional peak in the spectrum.

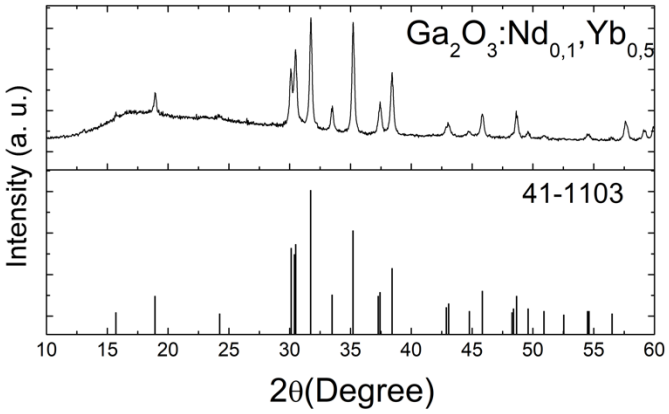

Figure 1. XRD pattern of Ga_2O_3:$Nd_{0,1}$, $Yb_{0,5}$ nanoparticles

Figure 2 shows the TEM image of Ga_2O_3:Yb^{3+}, Nd^{3+} nanoparticles. The prepared nanoparticles present spherical morphology and their size distribution is uniform with an average diameter of ~100-500 nm.

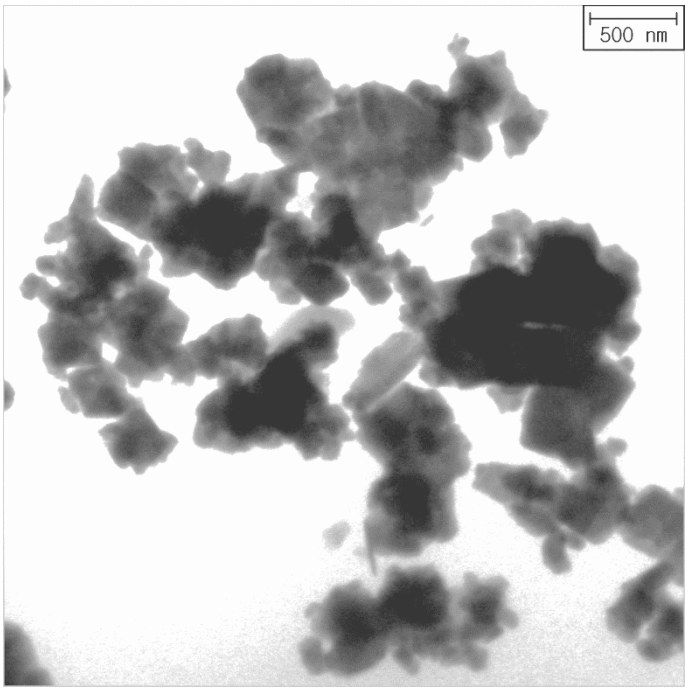

Figure 2. TEM image of Ga_2O_3:$Nd_{0,1}$, $Yb_{0,5}$ nanoparticles

3.2. Photoluminescence Properties of Ga_2O_3:Yb^{3+}, Nd^{3+} Nanoparticles

The room temperature photoluminescence emission spectrum of Ga_2O_3:Yb^{3+}, Nd^{3+} nanoparticles in the infrared region (900 -1400 nm) is shown in Figure 3. The 325 nm line of the He-Cd laser (10 mW) is used for sample excitation. PL emission spectrum consist of emission bands centered at 968 and 1070 nm. The band located at 968 nm has been associated with the $^2F_{5/2}\rightarrow{}^2F_{7/2}$ transition of Yb^{3+} ion, while the second emission band located at 1070 nm can be attributed to $^4F_{3/2}\rightarrow{}^4I_{9/2}$ transition of Nd^{3+} ion. It should be noticed that no clear emission is observed below ~900 nm due to the low sensitivity of the detector. Concentration of Nd^{3+} is fixed to 0,1 mol% and concentration of Yb^{3+} is varied from 0,4 to 0,5 mol% to understand energy transfer between Nd^{3+} and Yb^{3+} ions in the Ga_2O_3 samples. As Yb^{3+} ion concentration is increased, average distance between Yb^{3+} and Nd^{3+} ions is decreased. Therefore, it is expected that Yb^{3+} emission relative to Nd^{3+} should be increased due to an increase in energy transfer or the probability of cross relaxations [17,18]. However, the lower emission intensity of Yb^{3+} at 968 nm can be attributed to low energy transfer efficiency of Ga_2O_3 host crystal or back energy transfer [18].

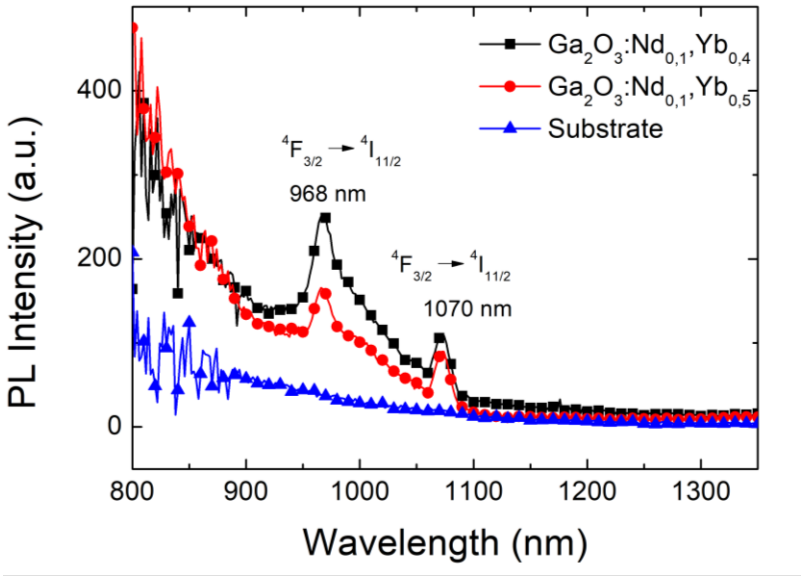

Figure 3. Photoluminescence emission spectrum of Ga_2O_3:Yb^{3+}, Nd^{3+} nanoparticles under 325 nm excitation

Figure 4 shows emission spectrum of Ga_2O_3:Yb^{3+}, Nd^{3+} nanoparticles under 477 nm wavelength laser excitation (~200 mW). Weak infrared emission bands are observed at 826, 876 nm (Nd^{3+}: $^4F_{3/2}\rightarrow{}^4I_{9/2}$), 968 nm ($Yb^{3+}$:$^2F_{5/2}\rightarrow{}^2F_{7/2}$), 1070 nm ($Nd^{3+}$: $^4F_{3/2}\rightarrow{}^4I_{11/2}$) and 1238, 1336 nm ($Nd^{3+}$: $^4F_{3/2}\rightarrow{}^4I_{13/2}$). As excitation wavelength is increased from 325 to 477 nm, Yb^{3+} emission intensity is decreased and Nd^{3+} emission intensity is increased. This emission intensity increase in Nd^{3+} can be attributed to the loss of one of the cross-relaxation channel leading to Yb^{3+} emission [13]. Besides, the peaks are weak and not sharp indicating the lower crystalline environment around the Nd^{3+} ions due to the lattice distortions that resulted from the large atomic radius difference between lanthanides (Yb, Nd) and Ga ions [14]

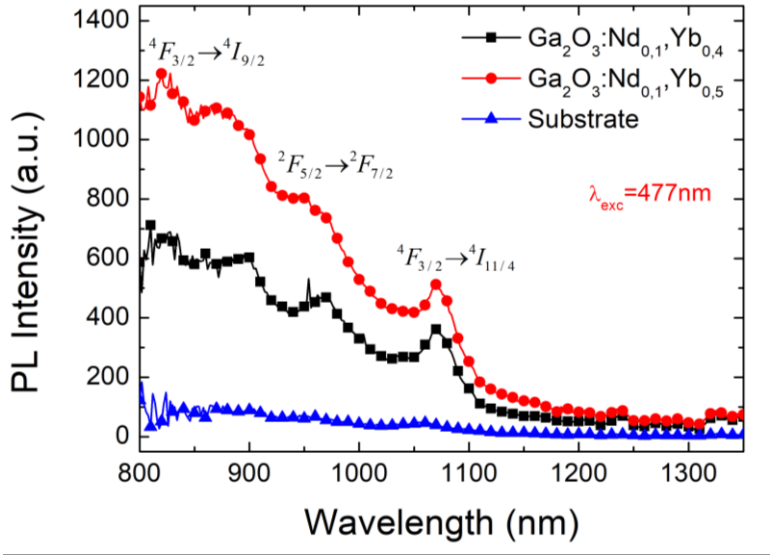

Figure 4. Photoluminescence Emission spectrum of Ga_2O_3: Nd^{3+}, Yb^{3+} nanoparticles under 477 nm excitation

The PL emission spectrum of Ga_2O_3: Nd^{3+}, Yb^{3+} nanoparticles under 515 nm wavelength laser excitation (~200 mW) is shown in Figure 5.

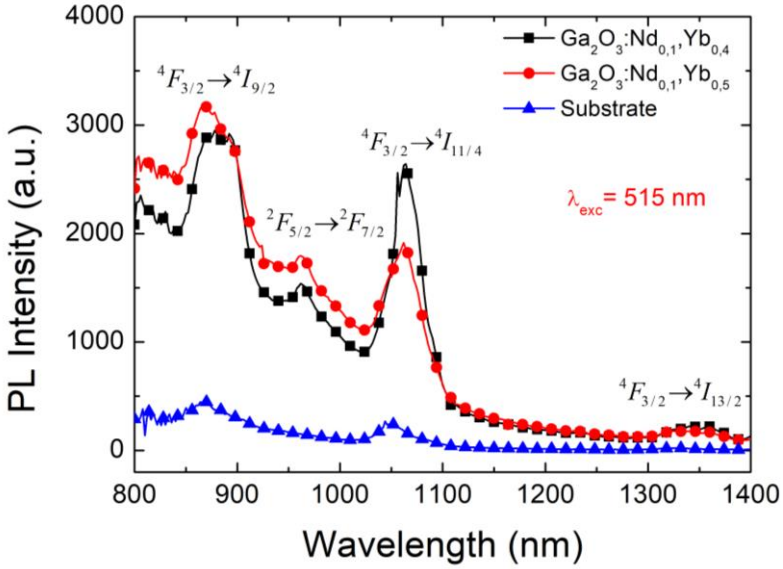

Three emission peaks observed at 868, 964 and 1070 nm corresponding to the Nd^{3+}: $^4F_{3/2}\rightarrow{}^4I_{9/2}$, Yb^{3+}:$^2F_{5/2}\rightarrow{}^2F_{7/2}$ and Nd^{3+}: $^4F_{3/2}\rightarrow{}^4I_{11/2}$, respectively. Multiple emission lines at 868 and 1070 nm are originated from the formation of stark sublevels due to the crystal field of Nd^{3+} ions [13,19] As the excitation wavelength is increased from 325 to 477 and 515 nm, Yb^{3+} emission peak intensity decreases while Nd^{3+} emission peak intensity increases. Also, another peak belongs to the Nd^{3+} ion at 1350 nm appears as the excitation wavelength is increased to 515 nm. This inverse relationship between the emission intensities of Yb^{3+} and Nd^{3+} ions indicates the presence of energy transfer between them [18]. Schematic representations of the energy level diagram describing possible energy transfer mechanism and transitions over the lanthanide ions in our sample is shown in Figure 6.

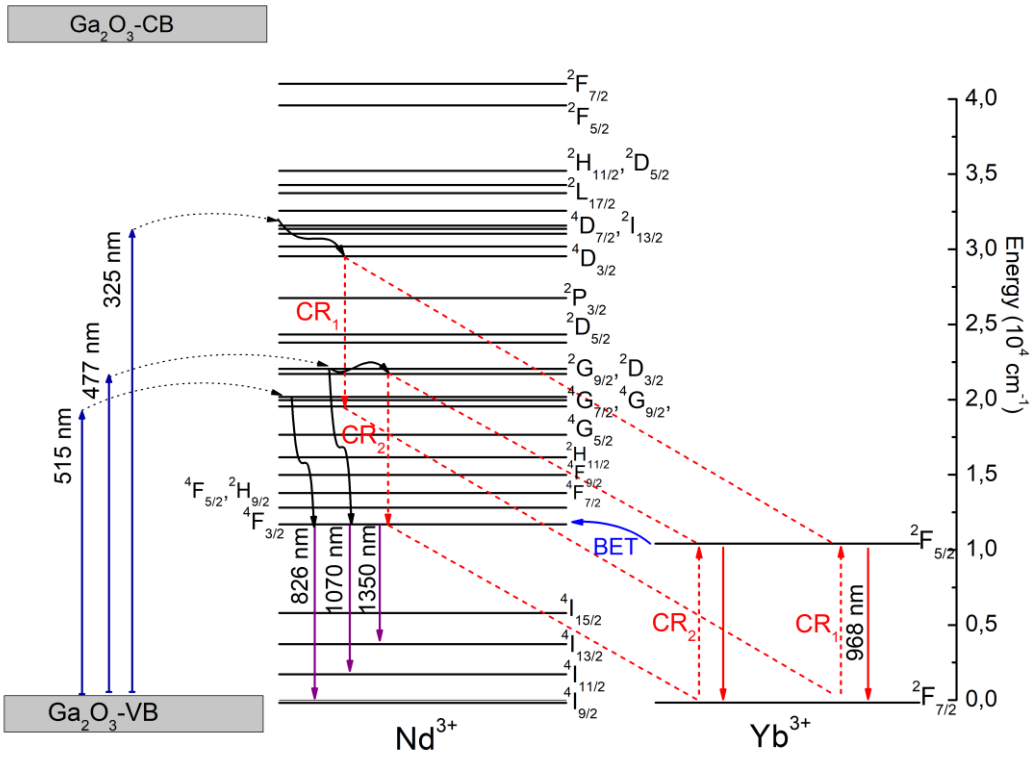

Figure 6. Schematic representations of the energy level diagram describing possible energy transfer mechanism

There are two possible ways for the excitation of lanthanide ions. The first possibility occurs via transitions throughout the electron trapped states within the band gap. The second one is the direct excitation of lanthanide ions via resonant energy transfer (Figure 6). One can find many examples in the literature explaining the energy transfer mechanisms in lanthanide-doped wide bandgap semiconductors. For example, Zhao et al. reported that excitation energy can be transferred to Eu^{3+} ions via electron traps in wide bandgap semiconductors, thereby leading to characteristic emissions of Eu^{3+} ion [20] . Bouras et al. claimed that the excitation of Nd^{3+} ions in the SnO_2 host crystal can occur either by (i) non-radiative energy transfer to the Nd^{3+} ions after band to band excitations of the SnO_2 host crystal or (ii) by electron traps within the bandgap [21]. In this study, the band gap of Ga_2O_3 is around 4,9 eV and its band to band excitation can be achieved at least with a 254 nm wavelength light source. Therefore, band to band excitation of present sample with 325 nm laser is not possible. Here, the optical property of the present samples seems to be controlled by electron traps. In general, a certain amount of oxygen vacancies are formed in semiconductor oxides depending on synthesis conditions [22–24] . These oxygen vacancies form empty energy levels below conduction band minimum (CBM), acting as electron traps. When Ga_2O_3: Nd^{3+}, Yb^3 nanoparticles are exposed to the 325 nm laser, electrons in the valence band are excited from the ground state to these electron traps. As soon as the electrons recombine with photogenerated holes, the resulting energy is transferred to the corresponding energy level of Nd^{3+} ions [25,26]. After multiphonon relaxations between $^4D_{7/2}$ and $^4D_{3/2}$ energy levels, there are two possibilities in the energy transfer process. First, electrons might decay from $^4D_{3/2}$ to $^4F_{3/2}$ energy levels of Nd^{3+} ions non-radiatively and then produce NIR emissions at 1070 nm via transitions between $^4F_{3/2}$ and $^4I_{11/2}$ energy levels. Second, electrons might transfer their energy to Yb^{3+} ions via CR1 cross-relaxations yielding emissions at 968 nm (Figure 6). It is difficult to talk about the existence of quantum cutting process here since the phonon energy of Ga_2O_3 is more than 500 cm^{-1} [18,27]. If so, the Yb^{3+} emission intensity should be the highest for high energy excitation (325 nm). When excitation wavelength increased to 477 nm, excited electrons in the $^2G_{9/2}$ energy level relax to $^4F_{3/2}$ energy level non-radiatively through both multiphonon and cross relaxations (CR2) resulting in weak emissions at 826, 876 nm (Nd^{3+}: $^4F_{3/2} \rightarrow {}^4I_{9/2}$),

968 nm (Yb^{3+}:$^2F_{5/2}\rightarrow{}^2F_{7/2}$), 1070 nm ($Nd^{3+}$: $^4F_{3/2}\rightarrow{}^4I_{11/2}$) and 1238, 1336 nm ($Nd^{3+}$:$^4F_{3/2}\rightarrow{}^4I_{13/2}$). But, as the energy levels are very close to each other between $^2G_{9/2}$ and $^4F_{3/2}$ levels, energy loss through the multiphonon relaxation reduces the energy transfer to Yb^{3+} ion. This may explain the reason for the decrease in Yb^{3+} emission compared to the 325 nm excitation (Figure 4). A strong Nd^{3+} and very weak Yb^{3+} emission are observed when the sample is excited with 515 nm laser irradiation. Compared to higher energy excitations (325 and 477 nm), Nd^{3+} emission intensity is the highest while Yb^{3+} emission intensity is the lowest (Figure 5). This could be originated from the loss of the CR1 and CR2 cross relaxations leading to Yb^{3+} emission. Besides, for all excitations (325, 477 and 515 nm), as Yb^{3+} concentration is increased the emission intensities of both Yb^{3+} and Nd^{3+} ions are decreased due to lattice distortions [18].

4. CONCLUSIONS

In summary, in order to understand the effects of defects (lanthanide dopants and oxygen vacancies) on the energy transfer mechanism, various excitation wavelengths and dopant concentrations experimented. As the excitation wavelength increased from 325 nm to 477 and 515 nm, Yb^{3+} emission peak intensity decreased while Nd^{3+} emission peak intensity increased. This inverse relationship between the emission intensities of Yb^{3+} and Nd^{3+} ion indicated the presence of energy transfer between them. However, it was observed that energy transfer from the host material was very weak due to lattice distortions and high phonon energies of Ga_2O_3 crystal. This result was deduced from the broad and weak emission peaks observed for each excitation wavelengths. The strongest Nd^{3+} emission was observed when the sample was resonantly pumped with 515 nm. This results indicate that Yb^{3+} and Nd^{3+} doped Ga_2O_3 can be used as imaging contrast agent for near infrared imaging applications in future.

CONFLICT OF INTEREST

The author stated that there are no conflicts of interest regarding the publication of this article.

REFERENCES

[1] Zhou J, Liu Z, Li F. Upconversion nanophosphors for small-animal imaging. Chem Soc Rev, 2012;41(3):1323-1349.

[2] Yu M, Li F, Chen Z, et al. Laser scanning up-conversion luminescence microscopy for imaging cells labeled with rare-earth nanophosphors. Anal Chem, 2009;81(3):930-935.

[3] Naccache R, Rodríguez EM, Bogdan N, et al. High resolution fluorescence imaging of cancers using lanthanide ion-doped upconverting nanocrystals. Cancers (Basel), 2012;4(4):1067-1105.

[4] Hong G, Antaris AL, Dai H. Near-infrared fluorophores for biomedical imaging. Nat Biomed Eng, 2017;1(1):0010.

[5] Wang C, Cheng L, Liu Z. Drug delivery with upconversion nanoparticles for multi-functional targeted cancer cell imaging and therapy. Biomaterials, 2011;32(4):1110-1120.

[6] Naczynski DJ, Tan MC, Zevon M, et al. Rare-earth-doped biological composites as in vivo shortwave infrared reporters. Nat Commun, 2013;4(1):2199.

[7] Smith AM, Mancini MC, Nie S. Second window for in vivo imaging. Nat Nanotechnol, 2009;4(11):710-711.

[8] Hong G, Lee JC, Robinson JT, et al. Multifunctional in vivo vascular imaging using near-infrared II fluorescence. Nat Med, 2012;18(12):1841-1846.

[9] Li Y, Zeng S, Hao J. Non-invasive optical guided tumor metastasis/vessel imaging by using lanthanide nanoprobe with enhanced down-shifting emission beyond 1500 nm. ACS Nano, 2019;13(1):248-259.

[10] Lim YT, Kim S, Nakayama A, Stott NE, Bawendi MG, Frangioni J V. Selection of quantum dot wavelengths for biomedical assays and imaging Mol Imaging, 2 (1): 50–64. Find this article online. Published online 2003.

[11] Diao S, Hong G, Antaris AL, et al. Biological imaging without autofluorescence in the second near-infrared region. Nano Res, 2015;8:3027-3034.

[12] Wang R, Li X, Zhou L, Zhang F. Epitaxial seeded growth of rare-earth nanocrystals with efficient 800 nm near-infrared to 1525 nm short-wavelength infrared downconversion photoluminescence for in vivo bioimaging. Angewandte Chemie International Edition, 2014;53(45):12086-12090.

[13] Talewar RA, Mahamuda S, Swapna K, Rao AS. Sensitization of Yb^{3+} by Nd^{3+} emission in alkaline-earth chloro borate glasses for laser and fiber amplifier applications. J Alloys Compd, 2019;771:980-986.

[14] Lupei A, Lupei V, Ikesue A, Gheorghe C, Hau S. Nd→ Yb energy transfer in (Nd, Yb): Y_2O_3 transparent ceramics. Opt Mater (Amst), 2010;32(10):1333-1336.

[15] Park J, An K, Hwang Y, et al. Ultra-large-scale syntheses of monodisperse nanocrystals. Nat Mater, 2004;3(12):891-895.

[16] Zhao J, Zhang W, Xie E, Ma Z, Zhao A, Liu Z. Structure and photoluminescence of β-Ga_2O_3: Eu3+ nanofibers prepared by electrospinning. Appl Surf Sci, 2011;257(11):4968-4972.

[17] Xia Z, Luo Y, Guan M, Liao L. Near-infrared luminescence and energy transfer studies of LaOBr: Nd^{3+}/Yb^{3+}. Opt Express, 2012;20(105):A722-A728.

[18] Borrero-González LJ, Nunes LA de O. Near-infrared quantum cutting through a three-step energy transfer process in Nd^{3+}–Yb^{3+} co-doped fluoroindogallate glasses. Journal of Physics: Condensed Matter, 2012;24(38):385501.

[19] Lupei V, Lupei A, Ikesue A. Spectroscopic properties of Nd^{3+} and highly efficient Nd^{3+} to Yb^{3+} energy transfer in transparent Sc_2O_3 ceramics. In: Advanced Solid-State Photonics. Optica Publishing Group, 2005;41.

[20] Jia Z, Arcangeli A, Tao X, et al. Efficient Nd^{3+}→ Yb^{3+} energy transfer in Nd 3+, Yb 3+: $Gd_3Ga_5O_{12}$ multicenter garnet crystal. J Appl Phys, 2009;105(8):083113.

[21] Bouras K, Rehspringer JL, Schmerber G, et al. Optical and structural properties of Nd doped SnO 2 powder fabricated by the sol–gel method. J Mater Chem C Mater, 2014;2(39):8235-8243.

[22] Liu Y, Luo W, Zhu H, Chen X. Optical spectroscopy of lanthanides doped in wide band-gap semiconductor nanocrystals. J Lumin, 2011;131(3):415-422.

[23] Kamiya T, Hosono H. Material characteristics and applications of transparent amorphous oxide semiconductors. NPG Asia Mater, 2010;2(1):15-22.

[24] Buckeridge J, Catlow CRA, Farrow MR, et al. Deep vs shallow nature of oxygen vacancies and consequent n-type carrier concentrations in transparent conducting oxides. Phys Rev Mater, 2018;2(5):054604.

[25] Wu Z, Bai G, Hu Q, et al. Effects of dopant concentration on structural and near-infrared luminescence of Nd^{3+}-doped beta-Ga_2O_3 thin films. Appl Phys Lett, 2015;106(17):171910.

[26] Chen Z, Wang X, Noda S, et al. Effects of dopant contents on structural, morphological and optical properties of Er doped Ga_2O_3 films. Superlattices Microstruct, 2016;90:207-214.

[27] Sun J, Sun Y, Cao C, Xia Z, Du H. Near-infrared luminescence and quantum cutting mechanism in $CaWO_4$: Nd^{3+}, Yb^{3+}. Applied Physics B, 2013;111:367-371.